Perovskite/Perovskite/Silicon Monolithic Triple-Junction Solar Cells with a Fully Textured Design

*Jérémie Werner,[1 *] Florent Sahli,[1] Fan Fu,[1] Juan J. Diaz Leon,[2] Arnaud Walter,[2] Brett A. Kamino,[2] Bjoern Niesen,[2] Sylvain Nicolay,[2] Quentin Jeangros,[1] and Christophe Ballif [1, 2]*

[1] Ecole Polytechnique Fédérale de Lausanne (EPFL), Institute of Microengineering (IMT), Photovoltaics and Thin-Film Electronics Laboratory, Rue de la Maladière 71b, 2002 Neuchâtel, Switzerland.

[2] CSEM, PV-Center, Jaquet-Droz 1, 2002 Neuchâtel, Switzerland

ABSTRACT

High efficiency triple-junction solar cells are currently made of III-V semiconductors using expensive deposition methods. Perovskite/perovskite/silicon monolithic triple-junction solar cells could be a lower cost alternative as no epitaxial growth is required. We demonstrate here that such devices can be realized using textured crystalline silicon bottom cells for optimal light management. By changing the perovskite absorbers composition and recombination junctions to make them compatible with the subsequent fabrication steps, triple-junction devices with open-circuit voltage up to 2.69 eV are realized using textured silicon wafers. To illustrate the applicability of the technology, we show how the band gaps and thicknesses of the top and middle cells can be modified to approach current-matching conditions. Current limitations of

these devices are discussed, as well as strategies to make them competitive with III-V triple-junction cells. The concepts presented here are a first step towards high-efficiency, high-voltage and low-cost triple-junction photovoltaics.

TOC GRAPHICS

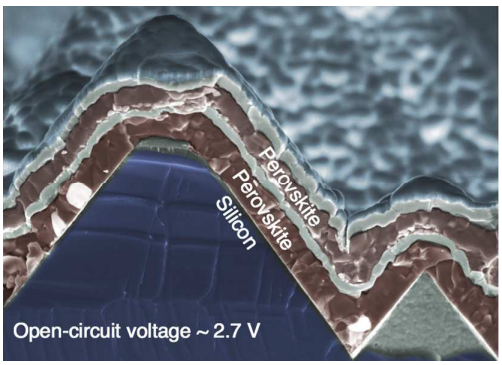

The photovoltaic market has massively grown and prices have consequently fallen over the last years.[1] As the costs of a photovoltaic system are now largely dominated by its installation and power electronics, e.g. inverters, increasing the power output at the cell and module levels is necessary to further drive down the costs of solar electricity. The most important losses in today's mainstream single-junction photovoltaic devices are linked to optical transparency and thermalization losses,[2] i.e. the absorber is transparent to photons with energies lower than its band gap and photons with energies higher than the band gap lose their excess energy through thermalization.

Multi-junction solar cells, where several absorbers with different band gaps are combined, offer the most straightforward solution to reduce these losses. With this strategy, the power-conversion efficiencies can be increased beyond the thermodynamic limit of single-junction solar cells[3]

through a more efficient use of the solar spectrum. Thanks to this high-efficiency potential, multi-junction solar cells have attracted a large interest in both academia and industry.[4–8]

III-V semiconductors have been used with success in multi-junction solar cells, achieving high efficiencies up to 38.8% for a 5-junction cell and 37.9% for a triple-junction solar cell (at 1 sun illumination intensity, i.e. 1000 W/m^2).[9] However, the metal organic chemical vapor deposition and molecular beam epitaxy techniques necessary to obtain high quality single crystals of such semiconductors are expensive,[10–12] prohibiting their application in large-scale terrestrial photovoltaic systems and hence restricting these technologies to space and high-concentration photovoltaic applications.

To lower the costs of multi-junction solar cells, attempts have been made to combine III-V materials with silicon (Si) technologies to profit from the large availability, low cost and narrow band gap of ~1.1 eV of the latter, a band gap well suited for a bottom cell. III-V/Si tandems have achieved an efficiency up to 32.8% in a 4-terminal configuration[7] and up to 33.3% in a wafer bonded triple-junction 2-terminal cell.[6] However, the applicability of 4-terminal mechanical stacks and 2-terminal cells made with wafer bonding is limited due to the complexity concerning system-level integration and the low throughput production process.[6] The direct growth of III-V materials on silicon would be preferred but is challenging to achieve due to the large lattice mismatch between these materials.[13] Efficiencies for such epitaxially-grown cells are so far limited to ~20%.[14]

Alternatively to this high efficiency but expensive technology, multi-junction solar cells have also been demonstrated with polycrystalline thin-film solar cells, such as thin-film silicon,[5,15–17] organic semiconductor,[18,19] or perovskite-based solar cells. However, among those options, only

perovskite solar cells exhibit both a high efficiency *and* the potential for low cost production. Thanks to their largely tunable band gap between 1.17 eV and >2 eV by compositional engineering,[20,21] their low processing temperature, enabled by a large defect tolerance,[22–24] they have already attracted a large interest for tandem applications. Experimentally demonstrated tandem architectures include perovskite/perovskite,[25–28] perovskite/chalcogenides[29,30] and perovskite/silicon[4,31–35] cells. For triple-junctions, the combination of two perovskite sub cells and a silicon bottom cell is likely the most attractive option due to its high efficiency potential of 38.8%, as predicted theoretically by Hörantner *et al.* using currently available materials properties.[36] Overall, the direct monolithic growth of high quality multi-crystalline materials such as perovskites on Si is intrinsically less challenging compared to the epitaxial growth of monocrystalline III-V materials.

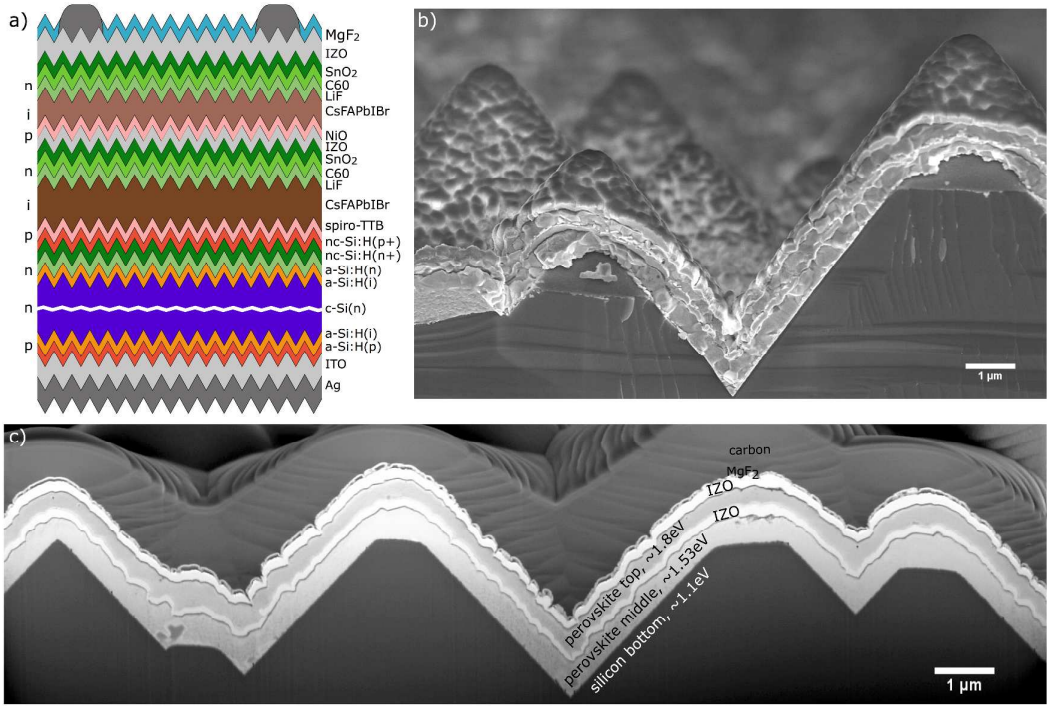

Figure 1: Device structure of triple-junction solar cells. a) Schematic view of a perovskite/perovskite/silicon heterojunction triple-junction solar cell and corresponding SEM images of b) cleaved and c) FIB-prepared cross-sections, showing that all layers are conformal, both for the middle and top cells. The white regions are the IZO middle and top electrodes. Carbon was deposited on top of the cell to protect the layer stack during the FIB sample preparation. Further SEM images can be found in the Supplementary Information (Figure S1).

Here, we present a proof-of-concept 2-terminal perovskite/perovskite/silicon triple-junction solar cell, which combines two perovskite cells grown monolithically onto a double-side textured crystalline silicon wafer and achieves an open circuit voltage close to 2.7 V. We experimentally show how slight variations in the top- and middle-cell absorber band gaps and thicknesses can help to approach an optimal current distribution. Next steps to improve the efficiency are also discussed.

The layer stack of the perovskite/perovskite/silicon triple-junction solar cells presented here is schematically shown in Figure 1a. Crystalline silicon wafers textured on both sides by alkaline etching, resulting in micron-sized pyramids, were used as bottom cells. This texture provides an optimized optical system by increasing light trapping and minimizing reflection effects, resulting in an increased performance compared to flat devices.[37,38] Using such double-side textured wafers, a certified efficiency of 25.2% was recently demonstrated for monolithic perovskite/silicon tandem solar cells.[39] Following this work on tandems, triple-junction cells were grown on double-side textured silicon heterojunction bottom cells with the n-type contact at the front. A nanocrystalline hydrogenated silicon (nc-Si:H) recombination junction was deposited by plasma-enhanced chemical vapour deposition (PECVD) at the front of the silicon heterojunction sub cell to form the interconnection with the middle cell. Previous studies demonstrated that this layer results in improved optical performance and electrical properties for the stack configuration presented here.[39,40]

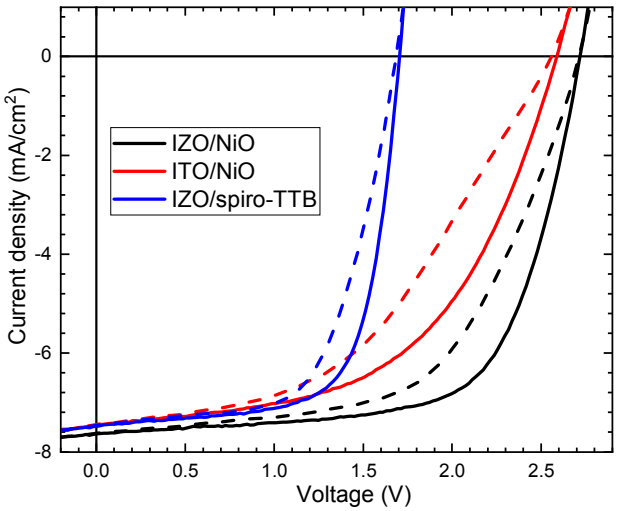

Figure 2: J-V measurements of triple-junction solar cells with either IZO/NiO, ITO/NiO or IZO/spiro-TTB as recombination junction and hole transporting layer between the middle and top sub cells. The corresponding J-V parameters are shown in Figure S2.

For the perovskite middle cell, a thermally evaporated 2,2',7,7'-tetra(N,N-di-tolyl)amino-9,9-spiro-bifluorene (spiro-TTB) layer was deposited directly on the p-type nc-Si:H layer to form the hole transport layer. The middle- and top-perovskite absorbers were grown using a sequential deposition method, as described in previous publications.[39,41] In brief, CsBr and PbI_2 were first co-evaporated to form a template layer. Then, either a formamidinium iodide solution for the middle cell or a formamidinium bromide solution for the top cell was spin coated onto the PbI_2/CsBr template, followed by thermal annealing in air to crystallize the perovskite phase. The $Cs_xFA_{1-x}Pb(I,Br)_3$ absorbers had optical band gaps (E_g) of ~1.53-1.55 eV and 1.77-1.8 eV for the middle and top cells, respectively. The electron contacts of both middle and top cells consisted of a thermally evaporated LiF/C_{60} stack,[42] completed by a SnO_2 buffer layer grown by atomic layer deposition (to reduce sputter damage) and a sputtered indium zinc oxide (IZO) or indium tin

oxide (ITO) electrode. Sputtered NiO was used as the hole transport layer for the top cell, as spiro-TTB was found to dewet transparent conductive oxides (TCOs) during the crystallization of the perovskite absorber, a process leading to a loss of charge carrier selectivity.[39] Indeed, the use of spiro-TTB as a hole transport layer in both the middle and top cells resulted in low voltages, around 1.7 V, similar to the values of a perovskite/silicon tandem cell (Figure 2). This suggests that, in these triple-junction cells, only the middle and bottom cells were contributing, in agreement with our previous findings on tandem cells.[39] More details about the device fabrication process can be found in the Experimental Methods section in the Supporting Information.

As shown in the cross-sectional scanning electron microscopy (SEM) images in Figure 1b and c, this approach enables the conformal deposition of all layers on the pyramidal surface texture of the silicon wafer. No signs of pin-holes or voids could be observed at this length-scale in the absorber layers, which were constant in thickness. The focused ion beam (FIB) cross-section shown in Figure 1c highlights the two IZO layers (white regions), which are used as the front electrode and the middle/top cell interconnection. The latter IZO layer does not only act as an effective recombination layer but also as a protective layer for the middle cell during the subsequent deposition of the top cell layers, as reported for perovskite/perovskite monolithic tandems.[25]

Using this combination of nc-Si:H and TCO recombination junctions, triple-junction cells were fabricated using standard cesium formamidinium lead halide compositions, initially with a E_g of ~1.77 eV for the top cell and of ~1.55 eV for the middle cell. These devices reached an open-circuit voltage (V_{oc}) close to 2.7 V, as shown in Figure 3a. Their efficiencies were limited however to around 12.7% during maximum power point tracking due to a low fill factor (FF).

The current density was severely limited by the middle cell, as indicated by the external quantum efficiency (EQE) measurements shown in Figure 3c. To improve the current distribution, the top cell absorption edge was then slightly blue-shifted to ~1.8 eV by increasing the Cs and Br contents, while the middle cell absorption edge was slightly red-shifted to ~1.53 eV by reducing the amount of Cs and Br in the perovskite layers (Figure 3b**)**. The top cell perovskite layer thickness was also reduced, further decreasing its absorption to increase the photocurrent in the middle cell. These modifications directly translated to a 1.9 mA/cm^2 gain in short-circuit current density (J_{sc}), improving from 7.7 to 9.6 mA/cm^2, as shown in Figure 3. This triple-junction cell had matched top- and middle-cell currents. However, these adaptations led to a lower FF, such that the maximum power point tracked efficiency only marginally improved to 13.2%.

The V_{oc}, demonstrated here, up to ~2.7 V, is below the expected sum of the individual sub cells. As the triple-junction cells were grown on textured wafers, it was not possible to co-deposit single-junction reference cells in the same configuration. We can however refer to our previous study on single-junction perovskite cells,[41] where V_{oc} values of ~1000 mV and ~1150 mV were demonstrated for perovskite absorbers with band gaps of ~1.53 eV and ~1.8 eV, respectively (cells with spiro-TTB and C_{60} as hole and electron charge transport layers, respectively). Assuming a contribution of ~650 mV from the silicon bottom cell, the triple cell should then show a V_{oc} close to 2.8 V. The lower experimental values can be explained by non-optimized recombination layers and limited optoelectronic quality of the thin wide-band gap top cell. Indeed, the lower $V_{oc,}$ FF and reduced EQE in the top/middle current-matched cell are likely linked to the lower quality of the top cell. Its thickness was reduced to optimize the J_{sc} but thinning this layer is likely to have resulted in the formation of shunts, i.e. regions with a direct contact between the charge carrier selective layers, as the perovskite coverage may have been

incomplete. A solution would be to further widen the band gap to >1.8 eV by replacing the evaporated PbI_2 precursor with $PbBr_2$ instead of reducing the thickness of the absorber. Overall, these optimizations should enable to achieve a V_{oc} of ~3.1 V, assuming that reported single-junction perovskite data[43–45] can be successfully transferred to triple cells.

As confirmed by the low reflectance (<3% between 400 nm and 1000 nm) shown in Figure 3c, the triple-junction cells exhibit good optical properties thanks to the high-aspect-ratio micron-sized pyramids of the silicon wafer.[39] The summed current density of all sub cells in the triple-junction device shown in Figure 3a is 38.8 mA/cm^2 without accounting for losses induced by the front-side metallization grid. This value indicates that parasitic absorption losses are relatively small (for comparison, record both-side-contacted Si cells achieve typically J_{sc} above 42.5 mA/cm^2 for 250 microns wafer).[9] This is encouraging considering the number of layers stacked in such a complex device. The remaining optical losses should still be reduced further by slightly thinning down the charge transport layers and/or replacing them with more transparent materials.[41] In addition, the summed current may be improved further by enhancing the optoelectronic quality of the perovskite absorber (e.g. the top cell of the device in Figure 3b) and hence charge carrier collection, and by improving the recombination junctions. In particular, the top/middle junction (now an IZO layer) could be replaced by an organic recombination junction, i.e. thin doped organic layers as demonstrated for perovskite/perovskite tandem cells.[27,28]

The main optimization path should however focus on tuning the band gaps and thicknesses of the top and middle perovskite cells. Indeed, the J_{sc} of a multi-junction solar cell with sub cells connected in series is dictated by the sub cell with the lowest current. To maximize the current generated by a triple-junction cell, the spectrum should be evenly distributed among its three sub cells. As seen in Figure 3, the current distribution is still far from optimal, as the bottom cell

produces a current density of about 18 mA/cm^2, twice as much as the perovskite sub cells. The absorption edge of the perovskite middle cell should be red-shifted to redistribute part of this excess current to the top and middle cells.

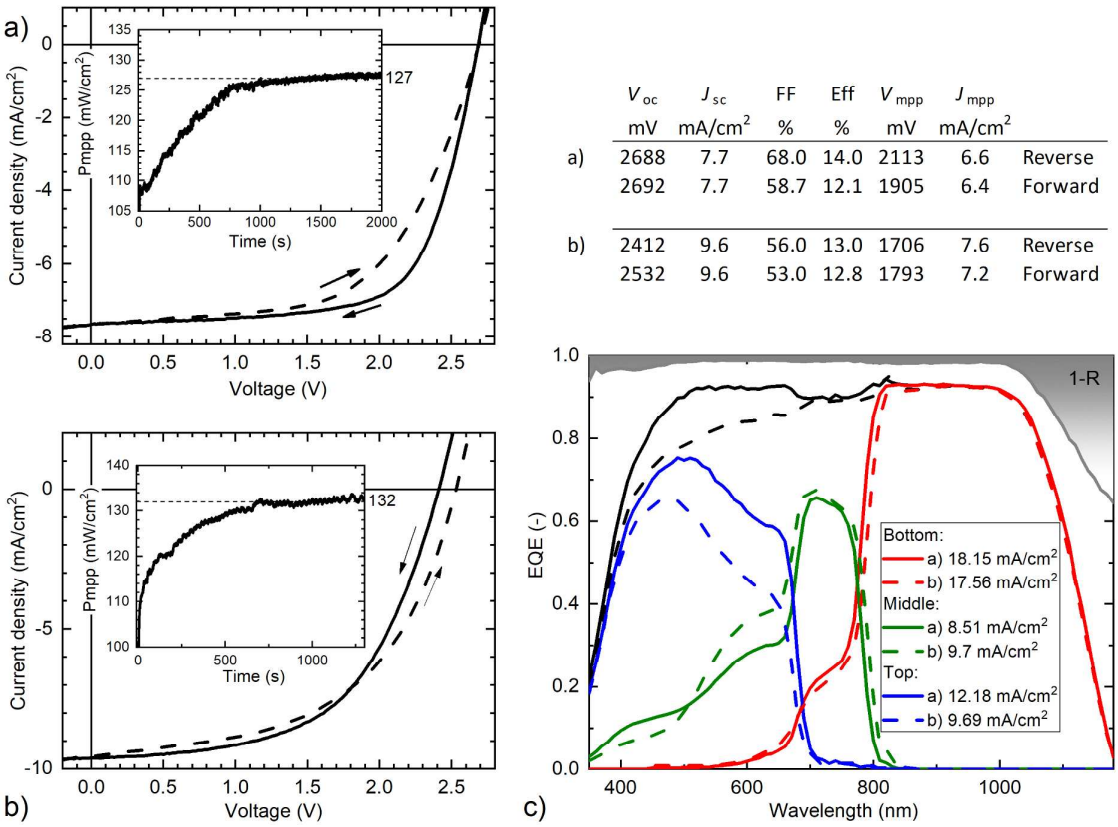

	V_{oc} mV	J_{sc} mA/cm^2	FF %	Eff %	V_{mpp} mV	J_{mpp} mA/cm^2	
a)	2688	7.7	68.0	14.0	2113	6.6	Reverse
	2692	7.7	58.7	12.1	1905	6.4	Forward
b)	2412	9.6	56.0	13.0	1706	7.6	Reverse
	2532	9.6	53.0	12.8	1793	7.2	Forward

Figure 3: J-V characteristics of triple-junction cells, with maximum power point tracking measurement as insets: a) with a top cell deposited with an evaporation rate of CsBr that is 13% of the one of PbI_2 (thickness of the CsBr/PbI_2 template of 250 nm, equivalent thickness on a flat glass substrate) and a middle cell with a 10% evaporation rate of CsBr and a template thickness of 400 nm; b) with a top cell of CsBr19%-180 nm and a middle cell of CsBr5%-450 nm. The corresponding J-V parameters are summarized in the table. The devices aperture area is 1.42 cm^2; c) EQE measurements of the cells shown in a) and b), showing how differences in band gaps in the top and middle cells and in thicknesses influence the current distribution, leading to a top/middle cell current-matched situation in b).

Transfer matrix optical simulations[41] were performed on all-flat structures (as a simplified model) to estimate ideal band gap and thickness ranges for our material stack configuration. The results are shown in Figure S3 and the method is explained in the Experimental Methods section. The simulations show that, considering a 1.8 eV top cell, the middle cell band gap should be lowered to ~1.4 eV. Using a flat silicon bottom cell, the triple cell can then be current-matched at ~12.2 mA/cm^2. This optimum corresponds also well to the ideal middle cell band gap inferred by the simulations from Hörantner *et al* using a different materials stack.[36] Note that when switching back to a double-side textured substrate, the large reflection losses observed in the simulations of flat devices will decrease, which should enable a J_{sc} >13 mA/cm^2 (the summed 38.8 mA/cm^2 shown in Figure 3c redistributed among the three sub cells, combined with expected improvements in carrier collection in the top and middle sub cells). The bottom cell will also likely gain proportionally more current than the two perovskite sub cells (i.e. infrared current),[31] which would push the requirement for the middle cell optimal band gap to even lower values. It should be noted that the current distribution should be tailored according to the specific application, e.g. terrestrial or spatial (see Figure S4). Furthermore, it should be mentioned that a perfect current-matched situation might not always lead to the highest device performance, as the FF is largely dictated by the current-limiting subcell.[46] Assuming that currently the Si sub cell should still yield the highest FF, a promising triple cell design should then aim for a slightly bottom cell-limited situation.

It is therefore clear that an important research effort is still required to yield a perovskite-based triple-junction cell with optimal band gaps and high performance. Significant progress was recently made on the development of wide band gap perovskite materials (>1.8 eV) with high V_{oc} (e.g. 1.35 V for a E_g of 1.85 eV).[47] Such values were achieved thanks to the use of additives to

standard compositions, notably large organic cations, as reviewed in Ref. [48] to mitigate/suppress the photo-induced phase segregation occurring in mixed halides compounds.[49] For the middle cell, fabricating high quality perovskite absorbers with band gaps <1.5 eV is still challenging. Several reports already demonstrated promising efficiencies of up to 17% (V_{oc} ~0.9V) with an absorption edge at 1.35 eV by substituting partially Pb with Sn.[21,50,51] These Pb-Sn perovskite properties are however usually synthesized with solution-based methods and exhibit a lower device performance when switching to the thermal evaporation routes that are required for textured surfaces.[52,53] If these low and high band gap perovskite materials demonstrated at the single junction level can be transposed to textured triple-junction cells, the 30% efficiency barrier could be surpassed with a current density of 13 mA/cm^2 (fully textured architecture), a V_{oc} of 3 V and a FF of 80%.

In summary, we demonstrated proof-of-concept triple-junction solar cells by monolithically growing two perovskite cells on double-side textured silicon wafers. The deposition methods, notably the evaporation/spin coating sequential process used to deposit the perovskite absorbers, enable the conformal growth of all the layer stack directly on the micron-sized pyramids of the Si bottom cell. The triple-junction devices fabricated here exhibit a V_{oc} of ~2.7 V. The equivalent cumulative current of 38.8 mA/cm^2 retrieved by summing the EQE current of the sub cells benefits from the presence of the pyramidal Si texture and is an evidence of the low parasitic absorption losses. We identified the next important development steps such as improving the current distribution by lowering the middle band gap to ~1.4 eV, optimizing the top/middle recombination junction and enhancing the V_{oc} of the wide-band gap front cell.[47] These preliminary results should open the research path towards high-efficiency, high-voltage and low-cost photovoltaic devices.

SUPPORTING INFORMATION

The Supporting Information is available free of charge on the ACS Publications website at DOI: XXXX.

Experimental methods for triple-junction cell fabrication; details on the device characterization; additional SEM cross-sectional images of flat and textured triple-junction cells; optical simulation data; spectral dependence of the photo-generated currents.

AUTHOR INFORMATION

Corresponding Author

*E-mail jeremie.werner@epfl.ch.

ACKNOWLEDGMENT

The authors thank Fabien Debrot and Christophe Allebé for SHJ wet-chemical processing, as well as Raphaël Monnard and Mathieu Boccard for the bottom cell deposition. This work was funded by the Nano-Tera.ch Synergy project, the Swiss Federal Office of Energy under Grant SI/501072-01, the Swiss National Science Foundation via the Sinergia Episode (CRSII5_171000) and NRP70 Energy Turnaround PV2050 (407040) projects and the European Union's Horizon 2020 research and innovation program under Grant Agreement No. 653296 (CHEOPS).

REFERENCES

(1) ITRPV. *International Technology Roadmap for Photovoltaic - 2016 Results*; 2017.

(2) Hirst, L. C.; Ekins-Daukes, N. J. *Prog. Photovoltaics Res. Appl.* **2011**, *19* (3), 286–293.

(3) Shockley, W.; Queisser, H. J. *J. Appl. Phys.* **1961**, *32* (3), 510–519.

(4) Werner, J.; Niesen, B.; Ballif, C. *Adv. Mater. Interfaces* **2018**, *5* (1), 1700731.

(5) Schüttauf, J.-W.; Niesen, B.; Löfgren, L.; Bonnet-Eymard, M.; Stuckelberger, M.; Hänni, S.; Boccard, M.; Bugnon, G.; Despeisse, M.; Haug, F.-J.; Meillaud, F.; Ballif, C. *Sol. Energy Mater. Sol. Cells* **2015**, *133*, 163–169.

(6) Cariou, R.; Benick, J.; Feldmann, F.; Höhn, O.; Hauser, H.; Beutel, P.; Razek, N.; Wimplinger, M.; Bläsi, B.; Lackner, D.; Hermle, M.; Siefer, G.; Glunz, S. W.; Bett, A. W.; Dimroth, F. *Nat. Energy* **2018**, *3* (4), 326–333.

(7) Essig, S.; Allebé, C.; Remo, T.; Geisz, J. F.; Steiner, M. A.; Horowitz, K.; Barraud, L.; Ward, J. S.; Schnabel, M.; Descoeudres, A.; Young, D. L.; Woodhouse, M.; Despeisse, M.; Ballif, C.; Tamboli, A. *Nat. Energy* **2017**, *2* (9), 17144.

(8) Ameri, T.; Dennler, G.; Lungenschmied, C.; Brabec, C. J. *Energy Environ. Sci.* **2009**, *2* (4), 347.

(9) Green, M. A.; Hishikawa, Y.; Dunlop, E. D.; Levi, D. H.; Hohl-Ebinger, J.; Ho-Baillie, A. W. Y. *Prog. Photovoltaics Res. Appl.* **2018**, *26* (7), 427–436.

(10) Bosi, M.; Pelosi, C. *Prog. Photovoltaics Res. Appl.* **2007**, *15* (1), 51–68.

(11) Bobela, D. C.; Gedvilas, L.; Woodhouse, M.; Horowitz, K. A. W.; Basore, P. A. *Prog. Photovoltaics Res. Appl.* **2017**, *25* (1), 41–48.

(12) Greenaway, A. L.; Boucher, J. W.; Oener, S. Z.; Funch, C. J.; Boettcher, S. W. *ACS Energy Lett.* **2017**, *2* (10), 2270–2282.

(13) Vaisman, M.; Fan, S.; Nay Yaung, K.; Perl, E.; Martín-Martín, D.; Yu, Z. J.; Leilaeioun, M.; Holman, Z. C.; Lee, M. L. *ACS Energy Lett.* **2017**, *2* (8), 1911–1918.

(14) Soga, T.; Kato, T.; Yang, M.; Umeno, M.; Jimbo, T. *J. Appl. Phys.* **1995**, *78* (6), 4196–4199.

(15) Multone, X.; Fesquet, L.; Borrello, D.; Romang, D.; Choong, G.; Vallat-Sauvain, E.; Charrière, M.; Billet, A.; Boucher, J.-F.; Steinhauser, J.; Orhan, J.-B.; Monnard, R.; Cardoso, J.-P.; Charitat, G.; Dehbozorgi, B.; Guillot, N.; Monteduro, G.; Marmelo, M.; Semenzi, R.; Benagli, S.; Meier, J. *Sol. Energy Mater. Sol. Cells* **2015**, *140*, 388–395.

(16) Si, F. T.; Isabella, O.; Tan, H.; Zeman, M. *Sol. RRL* **2017**, *1* (3–4), 1700036.

(17) Liu, B.; Bai, L.; Li, T.; Wei, C.; Li, B.; Huang, Q.; Zhang, D.; Wang, G.; Zhao, Y.; Zhang, X. *Energy Environ. Sci.* **2017**, *10* (5), 1134–1141.

(18) Sista, S.; Hong, Z.; Chen, L.-M.; Yang, Y. *Energy Environ. Sci.* **2011**, *4* (5), 1606.

(19) Ameri, T.; Li, N.; Brabec, C. J. *Energy Environ. Sci.* **2013**, *6* (8), 2390.

(20) Noh, J. H.; Im, S. H.; Heo, J. H.; Mandal, T. N.; Seok, S. I. *Nano Lett.* **2013**, *13* (4), 1764.

(21) Hao, F. .; Stoumpos, C. C.; Chang, R. P. H.; Kanatzidis, M. G. *J. Am. Chem. Soc.* **2014**, *136* (22), 8094–8099.

(22) De Wolf, S.; Holovský, J.; Moon, S. J. S.-J.; Löper, P.; Niesen, B.; Ledinsky, M.; Haug, F.-J. F. J.; Yum, Y.-H.; Ballif, C.; Holovsky, J.; Moon, S. J. S.-J.; Löper, P.; Niesen, B.; Ledinsky, M.; Haug, F.-J. F. J.; Yum, J. H.; Ballif, C. *J. Phys. Chem. C* **2014**, *5* (6), 1035–1139.

(23) Walsh, A.; Scanlon, D. O.; Chen, S.; Gong, X. G.; Wei, S. *Angew. Chemie Int. Ed.* **2015**, *54* (6), 1791–1794.

(24) Lee, J.-W.; Bae, S.-H.; De Marco, N.; Hsieh, Y.-T.; Dai, Z.; Yang, Y. *Mater. Today Energy* **2018**, *7*, 149–160.

(25) Eperon, G. E. G. E.; Leijtens, T.; Bush, K. A. K. A.; Prasanna, R.; Green, T.; Wang, J. T.-W. J. T.-W. J. T. W.; McMeekin, D. P. D. P.; Volonakis, G.; Milot, R. L. R. L.; May, R.; Palmstrom, A.; Slotcavage, D. J. D. J.; Belisle, R. A. R. A.; Patel, J. B. J. B.; Parrott, E. S. E. S.; Sutton, R. J. R. J.; Ma, W.; Moghadam, F.; Conings, B.; Babayigit, A.; Boyen, H. H.-G.; Bent, S.; Giustino, F.; Herz, L. M. L. M.; Johnston, M. B. M. B.; McGehee, M. D. M. D.; Snaith, H. J. H. J. *Science (80-.).* **2016**, *354* (6314), 861–865.

(26) Zhao, D.; Wang, C.; Song, Z.; Yu, Y.; Chen, C.; Zhao, X.; Zhu, K.; Yan, Y. *ACS Energy Lett.* **2018**, *3* (2), 305–306.

(27) Sheng, R.; Hörantner, M. T.; Wang, Z.; Jiang, Y.; Zhang, W.; Agosti, A.; Huang, S.; Hao, X.; Ho-Baillie, A.; Green, M.; Snaith, H. J. *J. Phys. Chem. C* **2017**, *121* (49), 27256–27262.

(28) Forgács, D.; Gil-Escrig, L.; Pérez-Del-Rey, D.; Momblona, C.; Werner, J.; Niesen, B.; Ballif, C.; Sessolo, M.; Bolink, H. J. *Adv. Energy Mater.* **2017**, *7* (8), 1–6.

(29) Fu, F.; Feurer, T.; Weiss, T. P.; Pisoni, S.; Avancini, E.; Andres, C.; Buecheler, S.; Tiwari, A. N. *Nat. Energy* **2016**, *2* (1), 16190.

(30) Fu, F.; Feurer, T.; Jäger, T.; Avancini, E.; Bissig, B.; Yoon, S.; Buecheler, S.; Tiwari, A.

N. *Nat. Commun.* **2015**, *6* (1), 8932.

(31) Werner, J.; Barraud, L.; Walter, A.; Bräuninger, M.; Sahli, F.; Sacchetto, D.; Tétreault, N.; Paviet-Salomon, B.; Moon, S.-J.; Allebé, C.; Despeisse, M.; Nicolay, S.; De Wolf, S.; Niesen, B.; Ballif, C. *ACS Energy Lett.* **2016**, *1* (2), 474–480.

(32) Bush, K. A.; Palmstrom, A. F.; Yu, Z. J.; Boccard, M.; Cheacharoen, R.; Mailoa, J. P.; McMeekin, D. P.; Hoye, R. L. Z.; Bailie, C. D.; Leijtens, T.; Peters, I. M.; Minichetti, M. C.; Rolston, N.; Prasanna, R.; Sofia, S.; Harwood, D.; Ma, W.; Moghadam, F.; Snaith, H. J.; Buonassisi, T.; Holman, Z. C.; Bent, S. F.; McGehee, M. D. *Nat. Energy* **2017**, *2* (4), 17009.

(33) Wu, Y.; Yan, D.; Peng, J.; Duong, T.; Wan, Y.; Phang, S. P.; Shen, H.; Wu, N.; Barugkin, C.; Fu, X.; Surve, S.; Grant, D.; Walter, D.; White, T. P.; Catchpole, K. R.; Weber, K. J. *Energy Environ. Sci.* **2017**, *10* (11), 2472–2479.

(34) Duong, T.; Wu, Y.; Shen, H.; Peng, J.; Fu, X.; Jacobs, D.; Wang, E.; Kho, T. C.; Fong, K. C.; Stocks, M.; Franklin, E.; Blakers, A.; Zin, N.; McIntosh, K.; Li, W.; Cheng, Y.; White, T. P.; Weber, K.; Catchpole, K. *Adv. Energy Mater.* **2017**, *7* (14), 1700228.

(35) Ramírez Quiroz, C. O.; Shen, Y.; Salvador, M.; Forberich, K.; Schrenker, N.; Spyropoulos, G. D.; Heumüller, T.; Wilkinson, B.; Kirchartz, T.; Spiecker, E.; Verlinden, P. J.; Zhang, X.; Green, M. A.; Ho-Baillie, A.; Brabec, C. J. *J. Mater. Chem. A* **2018**, *6* (8), 3583–3592.

(36) Hörantner, M. T.; Leijtens, T.; Ziffer, M. E.; Eperon, G. E.; Christoforo, M. G.; McGehee, M. D.; Snaith, H. J. *ACS Energy Lett.* **2017**, *2* (10), 2506–2513.

(37) Santbergen, R.; Mishima, R.; Meguro, T.; Hino, M.; Uzu, H.; Blanker, J.; Yamamoto, K.; Zeman, M. *Opt. Express* **2016**, *24* (18), A1288.

(38) Altazin, S.; Stepanova, L.; Werner, J.; Niesen, B.; Ballif, C.; Ruhstaller, B. *Opt. Express* **2018**, *26* (10), A579.

(39) Sahli, F.; Werner, J.; Kamino, B. A.; Bräuninger, M.; Monnard, R.; Paviet-Salomon, B.; Barraud, L.; Ding, L.; Diaz Leon, J. J.; Sacchetto, D.; Cattaneo, G.; Despeisse, M.; Boccard, M.; Nicolay, S.; Jeangros, Q.; Niesen, B.; Ballif, C. *Nat. Mater.* **2018**, DOI:10.1038/s41563-018-0115-4.

(40) Sahli, F.; Kamino, B. A.; Werner, J.; Bräuninger, M.; Paviet-Salomon, B.; Barraud, L.; Monnard, R.; Seif, J. P.; Tomasi, A.; Jeangros, Q.; Hessler-Wyser, A.; De Wolf, S.; Despeisse, M.; Nicolay, S.; Niesen, B.; Ballif, C. *Adv. Energy Mater.* **2018**, *8* (6), 1701609.

(41) Werner, J.; Nogay, G.; Sahli, F.; Yang, T. C.-J.; Bräuninger, M.; Christmann, G.; Walter, A.; Kamino, B. A.; Fiala, P.; Löper, P.; Nicolay, S.; Jeangros, Q.; Niesen, B.; Ballif, C. *ACS Energy Lett.* **2018**, *3* (3), 742–747.

(42) Stolterfoht, M.; Wolff, C. M.; Márquez, J. A.; Zhang, S.; Hages, C. J.; Rothhardt, D.; Albrecht, S.; Burn, P. L.; Meredith, P.; Unold, T.; Neher, D. *Nat. Energy* **2018**, DOI:10.1038/s41560-018-0219-8.

(43) Tress, W. *Adv. Energy Mater.* **2017**, *7* (14), 1602358.

(44) Wolff, C. M.; Zu, F.; Paulke, A.; Toro, L. P.; Koch, N.; Neher, D. *Adv. Mater.* **2017**, *29*

(28), 1–8.

(45) Longo, G.; Momblona, C.; La-Placa, M.-G.; Gil-Escrig, L.; Sessolo, M.; Bolink, H. J. *ACS Energy Lett.* **2018**, *3* (1), 214–219.

(46) Bonnet-Eymard, M.; Boccard, M.; Bugnon, G.; Sculati-Meillaud, F.; Despeisse, M.; Ballif, C. *Sol. Energy Mater. Sol. Cells* **2013**, *117*, 120–125.

(47) Rajagopal, A.; Stoddard, R. J.; Jo, S. B.; Hillhouse, H. W.; Jen, A. K.-Y. *Nano Lett.* **2018**, *18* (6), 3985–3993.

(48) Yang, T. C.-J.; Fiala, P.; Jeangros, Q.; Ballif, C. *Joule* **2018**, DOI:10.1016/j.joule.2018.05.008.

(49) Hoke, E. T.; Slotcavage, D. J.; Dohner, E. R.; Bowring, A. R.; Karunadasa, H. I.; McGehee, M. D. *Chem. Sci.* **2015**, *6* (1), 613–617.

(50) Yang, Z.; Rajagopal, A.; Chueh, C.-C.; Jo, S. B.; Liu, B.; Zhao, T.; Jen, A. K.-Y. *Adv. Mater.* **2016**, *28* (40), 8990–8997.

(51) Yang, Z.; Rajagopal, A.; Jen, A. K. Y. *Adv. Mater.* **2017**, *29* (47), 1–7.

(52) Guo, F.; Lu, Z.; Mohanty, D.; Wang, T.; Bhat, I. B.; Zhang, S.; Shi, S.; Washington, M. A.; Wang, G.-C.; Lu, T.-M. *Mater. Res. Lett.* **2017**, *5* (8), 540–546.

(53) Yu, Y.; Zhao, D.; Grice, C. R.; Meng, W.; Wang, C.; Liao, W.; Cimaroli, A. J.; Zhang, H.; Zhu, K.; Yan, Y. *RSC Adv.* **2016**, *6* (93), 90248–90254.